JOURNAL OF COMPUTATIONAL PHYSICS 103, 390–401 (1992)

Hybrid Combinations of Global and Local Operators for Solving Helmholtz and Poisson Equations

I-TAI LU

Department of Electrical Engineering, Weber Research Institute, Polytechnic University, Farmingdale, New York 11735

H. K. JUNG

Department of Electrical Engineering, Kangwean National University, Chuncheon, Kangweando, Korea

AND

C. M. TSAI

Department of Electrical Engineering, Weber Research Institute, Polytechnic University, Farmingdale, New York 11735

Received February 15, 1991

This paper addresses hybrid methods which employ analytic or asymptotic approaches as global operators and which employ numerical algorithms as local operators for studying physical phenomena in complex environments governed by Helmholtz and Poisson equations. Specifically, a ray–mode–boundary elements–finite elements method for analyzing wave scattering from a scatterer embedded in a waveguid is shown. This hybrid method can also be employed to analyze static problems as the source frequency becomes zero. Numerical results show smooth transition between static and dynamic responses.

I. INTRODUCTION

No one single solution method can work satisfactorily to analyze physical phenomena in complex environments governed by the Helmholtz or Poisson equation for a broad range of parameters. Therefore, it may be advantageous to combine various approaches into a single framework, which will provide numerical efficiency and physical insight. Moreover, comparing the results from different hybrid combinations may provide validity checks for a complex problem. Though the physical phenomena of a dynamic system (governed by the Helmholtz equation) and those of a static system (governed by the Poisson equation) are quite different, frameworks of mathematical approaches for both systems are very similar to each other. In fact, many algorithms solving for the Helmholtz equation allow the source frequency to approach zero. Thereby, they can also solve for the Poisson equation without major modifications. In this paper we will discuss hybrid methods combining global and local operators to analyze both dynamic and static results for problems involving small obstacles embedded in a global environment.

In the Helmholtz or Poisson equation, we have three configurational coordinates. The most general hybrid method can be constructed by partitioning entire regions into subregions. In every subregion each configurational coordinate defines a local spectral domain. (Only evanescent spectra exist in a static system.) The solution in the subregion can then be solved in the original coordinate system, transformed domain, or mixed (phase) domain. Furthermore, there are various ways of partitioning spectra and of performing inverse transforms. Therefore, there usually exist many solution methods available for each subregion, and the proper options must be chosen to provide physical insight and to ensure numerical efficiency and accuracy. (Hybrid methods may be desirable even in some subregions.) To integrate various methods in these subregions, we impose boundary conditions at the interfaces between subregions. The field variables along these interfaces are then formulated in terms of system equations which are to be solved numerically. Efficient iterative schemes for solving the system equations are available when the coupling among subsystems is weak.

Regarding the dynamic analyses, typical global propagators of the environment, local scattering operators of the scatterer, and a systematic way of combining them are discussed in Section II. Section III describes a specific example which employs a ray–mode–boundary elements–finite elements method to analyze wave scattering by obstacles in a waveguide. The boundary element method is employed to

0021-9991/92 $5.00

model the coupling between the interior and the exterior of the scatterer, the finite element method to formulate the interior responses of the scatterer, and the ray–mode method to provide Green's function of the waveguide. The efficiency of the ray–mode Green's function makes use of the boundary–finite element method practical in waveguides, and the flexibility of the boundary–finite elements method permits the application of the Green's function considered to arbitrarily shaped and placed scatterers.

As the frequency approaches zero, the dynamic behaviors become static, and the Helmholtz equation is reduced to the Poisson equation. In the static limit the fields can no longer propagate, and the effective coupling or interaction ranges are greatly reduced. However, one may still need hybrid combinations of various methods to analyze a complex system if the coupling or interaction effects are not negligible. In Section IV, various methods discussed in Sections II and III are examined when the source frequency (f) approaches zero. Numerical simulations of both static and dynamic responses for various structures are presented in Section V. The transition of physical phenomena from the dynamic case ($f \neq 0$) to the static situation ($f = 0$) is closely examined. Conclusions are made in Section VI.

II. BRIEF OVERVIEW OF HYBRID METHODS FOR DYNAMIC RESPONSES

To solve the Helmholtz equation in a complex medium, analytic methods (such as spectral integration, mode expansion, generalized ray expansion, and ray–mode combination) are efficient global propagators for large structures but work only for separable geometries. Approximate approaches are more flexible than analytic techniques but are restricted to some asymptotic regimes, and it is difficult to assess the accuracy of the computed results. For example, high frequency methods, such as asymptotic ray theory and Gaussian beam method, are flexible enough to be adapted to non-planar and inhomogeneous layered media, but fail when media properties vary rapidly. Numerical algorithms are flexible operators for modeling any geometries but are inefficient global propagators. For example, low frequency methods, such as method of moments, T-matrix, finite elements, boundary elements, and finite difference, are convenient for small size structures, but are too computer intensive for large media. Therefore, we would like to combine various methods to utilize their advantages and avoid their disadvantages. In this section, we give a brief overview of global propagators, local scattering operators, and hybrid combinations of them.

A. *Global Propagators*

For propagation in a stratified medium, discrete or continuous transforms can be applied to the lateral coordinates. The remaining transverse coordinate can then be solved by numerical methods (such as finite elements and finite difference), analytic methods (such as characteristic Green's functions, invariant embedding, reflectivity, propagator), or asymptotic methods (such as WKBJ). Therefore, many alternative numerical schemes are available. According to the techniques employed for the three configurational coordinates, we have spectra–finite elements [1], spectra–finite difference [2], depth mode–lateral ray [3], etc. According to the ways of partitioning spectra and of performing inverse transform(s), we have spectral integral, mode, generalized ray, ray–mode [4, 5], etc.

In the generalized ray representation the field is resolved into progression (traveling) waves along (ray) trajectories that chart the local progress of the motion via multiple reflections and refractions between source and observer. When observation is made at the source point, separation of the singular contribution, i.e., the direct ray term, is very convenient for this ray representation. This scheme becomes intractable for large source–observer separation, where many rays must be included. When many layers are present, ray proliferation could be serious even for small source–observer separation.

The spectral integration approach highlights the features associated with the various plane waves (propagating and evanescent) that synthesize the source distribution. It represents all of the rays collectively and, therefore, can alleviate the difficulties of the ray proliferation. This method becomes inefficient at high frequencies and/or for large source–observer separation due to the strong oscillatory behavior of the integrand.

The modal expansion represents the field globally in terms of normal modes which propagate with different velocities in the direction parallel to the layers. It becomes inefficient at high frequencies and/or small source–observer separation, where many modes are required.

These three conventional approaches for the Green's function of a layered structure have complementary properties. None of them are satisfactory over a broad range of parameter regimes. Realizing that spectral intervals containing clusters of rays or modes are sparsely filled by modes or rays, respectively, the hybrid ray–mode method combines rays, modes, and remainders self-consistently within a single framework, so as to optimize the advantages of each. Here the remainders are actually modified spectral representations accounting for truncation effects of ray or mode series and are represented by partial sums of plane waves with complex spectra. This hybrid solution has advantages of the three conventional representations, i.e., separation of the singular term, remedy of the difficulties due to the ray proliferation or mode clustering, and efficiency for all possible arrangements of source and receiver locations. In some parameter regimes, the general hybrid ray–mode representation may reduce to one, or a

combination of two, of the three conventional representations, when the reduced form is more convenient.

If the medium properties are not laterally invariant, the exact transform theory fails. Nevertheless, local modes [6], intrinsic modes [7], asymptotic rays [8], paraxial beams [8, 9], and the adiabatic transform [10] are still useful in a weakly range-dependent medium. Some semi-numerical methods, such as parabolic equation [11], are also available. The parabolic equation method is an efficient approach for wave propagation problems in range-dependent environments because it replaces the reduced wave equation, which is a boundary value problem, with an initial value problem. A significant amount of work has been devoted to improve the accuracy of this algorithm.

When the medium does not have a preferential direction, the guided mode concept is no longer useful. However, the local plane wave spectra, such as asymptotic rays and paraxial beams [8, 9], remain useful if, except across interfaces, the variations of the medium properties occur over a scale length much larger than the wavelength. The beam algorithm consists of approximating a given source by a fan of beams and tracing the propagation of these beams through the environment. This method has the advantage of being free of certain ray-tracing artifacts such as perfect shadows and infinite field at caustics. It also obviates the need for searching the eigenray. The approach is particularly useful when other global propagators are not practical alternatives.

B. *Scattering Operators*

If the size of the scatterer is small, discrete coordinate methods such as finite difference and finite elements are suitable for modeling the interior responses. Coupling between the interior and exterior can be solved numerically by the boundary element or moment method. Both boundary elements and finite elements are discrete coordinate techniques, but they have complementary properties. The finite element method has the advantages that it can be applied to nonlinear and/or inhomogeneous media easily, and its coefficient matrices, which are sparse, may be arranged to be banded, symmetric, and diagonally dominant. The main disadvantage is that the unknowns must be of interest in the whole computing region. On the other hand, the boundary element method has the advantage that the unknowns can be solved only for some boundaries which may be far apart. However, it cannot be employed to analyze nonlinear and/or inhomogeneous media easily. It also yields full coefficient matrices. A hybrid combination of these two methods have been employed to analyze wave scattering by inhomogeneous scatterers embedded in a global environment.

TABLE I

Hybrid Combinations of Global Propagators and Local Operators

Geometric structures				
Global environments	Local obstacles	System equations	Algorithms	References
Layered media	Impenetrable, homogeneous, or inhomogeneous scatterers	Laplace and/or Poisson's equations	Image-mode-moment method	[12]
Layered media	Impenetrable, homogeneous, or inhomogeneous scatterers	Transient wave equation	Ray-mode-boundary elements-finite difference	[13]
Layered media	Impenetrable, homogeneous, or inhomogeneous scatterers	Helmholtz equations	Ray-mode-boundary elements	[14]
Layered media	Impenetrable, homogeneous, or inhomogeneous scatterers	Helmholtz equations	Ray-mode-boundary elements-finite elements	[15]
Layered media	Apertures	Helmholtz equations	Ray-mode-moment method	[16]
Cavity	Apertures	Helmholtz equations	Mode-moment method	[17]
Laminated materials	Flaws	Elastodynamic equations	Beam-mode-Born's approximation	[18]

C. *Combination of Global Propagators and Local Scattering Operators*

By imposing the boundary conditions on the surface of a scatterer, the global propagator and scattering operator will be integrated together. One way of doing so is to formulate the problem in terms of integral equations by invoking Green's theorem. By expressing the unknown field distributions along the scattering surface in terms of appropriate basis functions, these integral equations are then discretized and reduced to algebraic equations that are solved numerically. In the integral equations, the exterior Green's function is evaluated in terms of global propagators, and the interior response is modeled by local scattering operators. The recently developed hybrid algorithms for solving various geometric structures, governed by different system equations, are listed in Table I. In particular, the ray–mode–boundary elements–finite element method is summarized in the next section.

III. AN EXAMPLE

For the waveguide with an embedded inhomogeneous scatterer in Fig. 1, we seek the solution to the two-dimensional Helmholtz equation

$$\left[\rho(\mathbf{r})\frac{\partial}{\partial x}\frac{1}{\rho}(\mathbf{r})\frac{\partial}{\partial x}+\rho(\mathbf{r})\frac{\partial}{\partial z}\frac{1}{\rho}(\mathbf{r})\frac{\partial}{\partial z}+k^2(\mathbf{r})\,\phi(\mathbf{r})\right]=-s(\mathbf{r}),\qquad \mathbf{r}=(x,z),\tag{1}$$

with continuity of ϕ and $(1/\rho)(\partial/\partial n)\phi$ as boundary conditions. Here k is the wavenumber, s describes the source distribution, $\mathbf{n}$ is a normal vector to a boundary, ρ is a medium property, and ϕ is a wave potential. A time dependence $e^{-i\omega t}$ has been assumed.

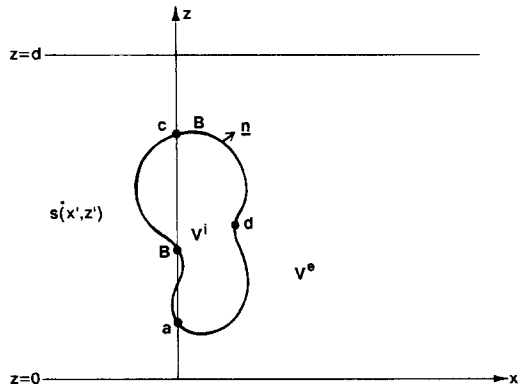

FIG. 1. An inhomogeneous scatterer embedded in a waveguide. B, V^e, and V^i represent the boundary, exterior, and interior of the scatterer, respectively. $\mathbf{n}$ is the normal vector to the boundary. (x', z') is the source location.

A. *Global Operator—Hybrid Ray–Mode Solution*

Consider the Green's function g of the homogeneous waveguide without the scatterer as the global operator. From (1) and Fig. 1, g satisfies the homogeneous wave equation

$$\left(\frac{\partial^2}{\partial x^2}+\frac{\partial^2}{\partial z^2}+k^2\right)g(\mathbf{r},\mathbf{r}')=-\delta(\mathbf{r}-\mathbf{r}'),\qquad \mathbf{r}=(x,z),\quad \mathbf{r}'=(x',z'),\tag{2}$$

and the boundary conditions at $z=0$ and d, which are described by the plane wave reflection coefficients R_0 and R_d, respectively. ($R_{0,d}=-1$ or 1 if $g=0$ or $\partial g/\partial n=0$, respectively.) The response to any source distribution $s(\mathbf{r})$ can then be evaluated by the superposition integral

$$\phi(\mathbf{r})=\int s(\mathbf{r}')\,g(\mathbf{r},\mathbf{r}')\,dV(\mathbf{r}').\tag{3}$$

The waveguide Green's function in (2) is represented in terms of a combination of rays, modes, and a remainder

$$g=\left[\sum_{l=1}^{4}\sum_{n=0}^{N-1}g_{nl}\right]_{\text{rays}}+\left[\sum_{m}^{M_N}g_m\right]_{\text{modes}}+[R_N]_{\text{remainder}},\tag{4}$$

where a typical ray of the lth species and with n reverberations is given by

$$g_{nl}=\frac{i}{4}A_{nl}H_0^{(1)}(kr_{nl}),\qquad r_{nl}=\sqrt{(x-x')^2+(z-z_{nl})^2},$$

$$A_{nl}=\begin{cases}(R_0R_d)^n, & l=1\\ R_0(R_0R_d)^n, & l=2\\ R_d((R_0R_d)^n, & l=3\\ (R_0R_d)^{n+1}, & l=4\end{cases}\tag{4a}$$

$$z_{nl}=\begin{cases}|z-z'|+2nd, & l=1\\ z+z'+2nd, & l=2\\ -z-z'+2(n+1)d, & l=3\\ -|z-z'|+2(n+1)d, & l=4\end{cases}$$

and the mth mode is specified by

$$g_m = \frac{i\alpha_m}{\zeta_m d}\sin(\kappa_m Z)\sin(\kappa_m Z')\exp[i\zeta_m|x-x'|],$$

$$\zeta_m = (k^2-\kappa_m^2)^{1/2}, \quad \mathrm{Im}(\zeta_m)\geq 0, \quad m=0, 1, 2, 3, \ldots;$$

$$\begin{cases} \alpha_m = 1, & \kappa_m = m\pi/d, \\ & Z' = z', \quad Z = z, \\ & \quad \text{if} \quad R_0 = -1, \quad R_d = -1 \\ \alpha_m = 1, & \kappa_m = (1/2+m)\,\pi/d, \\ & Z = d-z, \quad Z' = d-z', \\ & \quad \text{if} \quad R_0 = 1, \quad R_d = -1 \\ \alpha_m = \begin{cases} 1, & m>0 \\ 0.5, & m=0 \end{cases}, & \kappa_m = m\pi/d, \\ & Z = z-\dfrac{\pi}{2\kappa_m}, \quad Z' = z'-\dfrac{\pi}{2\kappa_m}, \\ & \quad \text{if} \quad R_0 = 1, \quad R_d = 1 \\ \alpha_m = 1, & \kappa_m = (1/2+m)\,\pi/d, \\ & Z = z, \quad Z' = z', \\ & \quad \text{if} \quad R_0 = -1, \quad R_d = 1. \end{cases} \tag{4b}$$

Playing a key role in determining the numbers of rays and modes, the remainder is defined as

$$R_N = \int_{C'} A(\zeta)\exp[iP(\zeta)]\,d\zeta, \tag{5}$$

where the phase term is

$$\begin{aligned} P(\zeta) &= 2N\kappa d + \zeta|x-x'|, \\ \kappa &= (k^2-\zeta^2)^{1/2}, \quad \mathrm{Im}(\kappa)\geq 0, \end{aligned} \tag{5a}$$

and the amplitude function is

$$A(\zeta) = \frac{\left[\begin{array}{c} e^{i\kappa|z-z'|} + R_0 e^{i\kappa(z+z')} + R_d e^{i\kappa(2d-(z+z'))} \\ + R_0 R_d e^{i\kappa(2d-|z-z'|)} \end{array}\right]}{-4\pi i\kappa(1-R_0 R_d e^{i2\kappa d})}. \tag{5b}$$

The integration contour C' is the steepest descent path in the complex ζ domain specified by the condition

$$P(\zeta) = P(\zeta_{sN}) + iu, \qquad u>0, \tag{6}$$

where ζ_{sN} is the saddle point

$$\zeta_{sN} = k|x-x'|\,[(2Nd)^2+(x-x')^2]^{-1/2}. \tag{6a}$$

The contour C' in (5) partitions the entire spectra into two parts which are to be accounted for by rays and modes, respectively. The mode sum in (4) is contributed from those modes g_m intercepted during the path deformation from the real axis C to the steepest descent contour C', and the ray sum in (4) is from those rays g_{nl} with n less than N. The ability of explicit separation of the direct ray g_{01} in (4) is important for evaluating the singular contribution in the boundary element method in Section III.C when source and receiver are overlapping each other. One criterion to determine the number N in (4) is related to how easy one can compute the remainder in (5), where a first-order asymptotic approximation, when possible, is preferred (see Appendix A). A rule of thumb is to keep the saddle point ζ_s away from pole ζ_m's (see (A1)) and to make sure that the amplitude is relatively a slowly varying function with respect to the phase (see (A2)). The other criterion of choosing N is to minimize the total number of rays and modes. If computing rays is much easier than computing modes or vice versa, one may try to minimize the number of rays or modes, respectively.

For sufficiently large N, the saddle point approaches zero and no modes will be intercepted (unless $\zeta=0$ is a pole of (5)). The hybrid ray–mode solution in (4) is reduced to the ray plus remainder solution,

$$g = \left[\sum_{l=1}^{4}\sum_{n=0}^{N-1} g_{nl}\right] + R_N, \tag{7}$$

where the remainder can be interpreted as a collective ray accounting for rays g_{nl} with $n\geq N$. If $N=\infty$, (4) is reduced to the conventional ray solution

$$g = \sum_{n=1}^{\infty}\sum_{l=0}^{4} g_{nl}. \tag{8}$$

If $N=0$, no saddle point exists for the phase in (5a). When choosing C' to be the real axis C, the hybrid ray–mode solution is reduced to the conventional plane wave spectral representation which is the same as the remainder integral in (5) by letting $N=0$ and $C'=C$.

Closing the integration path C by a semicircle at infinity and employing the residue theorem, the ray–mode solution is reduced to the conventional modal solution

$$g = \sum_{m=0}^{\infty} g_m. \tag{9}$$

Since the separation of amplitude and phase in a spectral

integral such as (5) is not unique, the steepest descent contour is also not unique. Therefore the number of modes included in (4) may depend on the definition of phase in (5a). No approximation is made so far, and the solution options in (4), (7), (8), or (9) are exact. This feature is very suitable for numerical implementation to optimize the computational efficiency. Since the mode sum converges slowly for small $|x-x'|$ and the ray sum converges slowly for large $|x-x'|$, it is suggested to predetermine three threshold values X_1, X_2, and X_3, $X_1 \leqslant X_2 \leqslant X_3$, where the mode, ray–mode, ray–remainder, and ray formats are employed for $X_3 < |x-x'|$, $X_3 \geqslant |x-x'| \geqslant X_2$, $X_2 \geqslant |x-x'| \geqslant X_1$, and $X_1 > |x-x'|$, respectively. The determination of X_i, $i=1, 2, 3$, depends on the computational efficiency of each individual term and the converging efficiency of these options. Fortunately small variation of these threshold values does not affect the accuracy or efficiency of the algorithm.

Since it takes almost the same amount of time to evaluate a ray (4a), a mode (4b), and the remainder (A3) for the present example, we will choose X_i, $i=1, 2, 3$, to minimize the terms required in computing the Green's function. In the following, we will estimate the minimum number of terms required in each option and then provide a simple formula to determine the X's. At first, approximate the total number of terms in the hybrid ray–mode solution (4) by

$$T_H \approx \text{Minimum}[4(N)+M_N]_{N\geqslant 5}+1,$$
$$M_N \approx \frac{d}{\pi}(k^2-\zeta_{sN}^2)^{1/2}. \tag{10}$$

Second, by noting that $|g_{nl}| < (8\pi k r_{nl})^{-1/2}$ and $r_{nl} \approx 2nd$ for large n, the total number of terms in the ray solution (8) is

$$T_R = 4\bar{N}+1,$$
$$\bar{N} \approx \frac{1}{16\pi k d\delta^2} \quad \text{when} \quad 2\bar{N}d \gg |x-x'|, \tag{11}$$

where δ is a pre-specified error tolerance ($|g_{nl}| < \delta$) and the infinite ray sum in (8) is truncated at $\bar{N}$. Regarding the ray plus ray remainder option, the number N in (7) can be approximated by (see (A1))

$$N \approx \frac{(P(\zeta_{M'})+5)}{2kd} \quad \text{when} \quad 2Nd \gg |x-x'|,$$
$$P(\zeta_s(N)) \approx 2kNd, \tag{12}$$

where $\zeta_{M'}$ is the smallest wavenumber of the propagating modes. Similar to the ray solution, the total number of terms T_{RR} in the ray–remainder solution is $4N+1$. Finally, the infinite mode sum can be truncated at T_M which can be estimated a priori by solving

$$\delta = \left(1\Big/d\left[\left(\frac{M'\pi}{d}\right)^2 - k^2\right]^{1/2}\right) \times \exp\left\{-\left[\left(\frac{T_M\pi}{d}\right)^2 - k^2\right]^{1/2}|x-x'|\right\}, \qquad T_M > M', \tag{13}$$

where δ is a pre-specified error tolerance ($|g_m|_{m=T_M} \leqslant \delta$), and M' is the total number of propagating modes. From (10)–(13), the threshold values are determined by

$$X_3 \approx (x-x' \mid T_M = T_H),$$
$$X_2 \approx (x-x' \mid T_H = T_{RR}),$$
$$X_1 \approx (x-x' \mid T_{RR} = T_R), \quad X_3 \geqslant X_2 \geqslant X_1 \geqslant 0. \tag{14}$$

If there is no solution for X_1, we choose X_1 to be zero if $T_R > T_{RR}$ and choose X_1 to be X_2 if $T_R < T_{RR}$. If there is no solution of X_2 we choose $X_2 = X_3$.

B. *Local Operator—Finite Element Method*

Since the inhomogeneous scatterer is confined in a local region, numerical approaches are suitable to analyze the internal response of the scatterer. In this paper, we will discuss only the finite element method which is very flexible and its coefficient matrices are sparse. The conventional finite element method proceeds by discretizing the interior of the scatterer into small elements. Let V_e denote the eth element of the scatterer and $\tilde{\phi}_e$ be an approximate solution of (1) in V_e. The corresponding residual is defined as

$$R_e = \left[\frac{\partial}{\partial x}\left(\frac{1}{\rho_e}\frac{\partial}{\partial x}\right)+\frac{\partial}{\partial z}\left(\frac{1}{\rho_e}\frac{\partial}{\partial z}\right)+\frac{k_e^2}{\rho_e}\right]\tilde{\phi}_e + \frac{s_e}{\rho_e}, \tag{15}$$

where the subscript "e" denotes the eth element. By invoking the weighted residual method, a sum of weighted volume integrals for the scatterer is set to zero to minimize the residuals,

$$\sum_{e=1}^{M}\int_{V_e} WR_e\, dV = 0, \tag{16}$$

where W is a weighting function and M is the number of

elements in the scatterer. Employing Green's formula, Eq. (16) becomes

$$\sum_{e=1}^{M}\left[\int_{V_e}\frac{1}{\rho_e}\left(\frac{\partial W}{\partial x}\frac{\partial\tilde{\phi}_e}{\partial x}+\frac{\partial W}{\partial z}\frac{\partial\tilde{\phi}_e}{\partial z}\right)dV-\int_{V_e}\frac{k_e^2}{\rho_e}W\tilde{\phi}_e\,dV-\int_{V_e}\frac{1}{\rho_e}Ws_e\,dV-\oint_{B_e}\frac{1}{\rho_e}W\frac{\partial}{\partial n}\tilde{\phi}_e\,dr_B\right]=0, \quad (17)$$

where B_e is the boundary of V_e and $\mathbf{n}$ is an outward normal to B_e. Since the surface integral along the interfaces of neighboring elements cancel each other, the sum of boundary integral terms of small elements in (17) is reduced to a sum of boundary integrals along the surface of the scatterer. The integral can be further discretized as

$$\sum_{e=1}^{M}\oint_{B_e}\frac{1}{\rho_e}W\frac{\partial\tilde{\phi}_e}{\partial n}dr_B=\oint_B\frac{1}{\rho}W\frac{\partial\tilde{\phi}}{\partial n}dr_B\approx\sum_{i=1}^{I}\left(\int_{\Delta B_i}\frac{1}{\rho}W\,dr_B\right)\frac{\partial}{\partial n}\tilde{\phi}(\mathbf{r}_i), \quad (18)$$

where r_i is the mid-point of the ith boundary element ΔB_i and I is the number of boundary elements of the scatterer. Here $\tilde{\phi}$ and ρ are the field and density, respectively, in the scatterer.

To discretize the volume integrals in (17) express the solutions

$$\tilde{\phi}_e(\mathbf{r})=\sum_j N_j(\mathbf{r})\,\phi_j, \quad (19)$$

where N_j is a known nodal shape function, and ϕ_j is an unknown nodal value of the jth node in the scatterer. The summation in (19) is *only* over the nodes of the eth element. Substituting (18) and (19) into (17) and by Galerkin's method choosing the nodal shape functions (N_j, $j=1, 2, ..., J$) to be the weighting function W, we obtain a matrix equation

$$E\Phi+F\Psi^b=S, \quad (20)$$

where Φ, Ψ^b, and S, respectively, are the nodal field, boundary field, and nodal excitation vectors:

$$\Phi=[\phi_j]_{J\times 1}, \qquad j=1, 2, ..., J, \quad (20a)$$

$$\Psi^b=\left[\frac{\partial}{\partial n}\phi(\mathbf{r}_i)\right]_{I\times 1}, \qquad i=1, 2, ..., I, \quad (20b)$$

$$S=[S_j]_{I\times 1}, \qquad S_j=\sum_e\int_{V_e}N_j\frac{s_e}{\rho_e}dV, \qquad j=1, 2, ..., J, \quad (20c)$$

E is the nodal coefficient matrix

$$E=[E_{ij}]_{J\times J}, \qquad i,j=1, 2, ..., J,$$
$$E_{ij}=\sum_e\int_{V_e}\frac{1}{\rho_e}\left[\frac{\partial N_i}{\partial x}\frac{\partial N_j}{\partial x}+\frac{\partial N_i}{\partial z}\frac{\partial N_j}{\partial z}-k_e^2N_iN_j\right]dV, \quad (20d)$$

and F is the boundary coefficient matrix

$$F=[F_{ij}]_{J\times I}, \qquad i,j=1, 2, ..., J,$$
$$F_{ij}=\int_{\Delta B_j}\frac{1}{\rho}N_i\,dr_B. \quad (20e)$$

The summation in (20c) is over elements adjacent to the jth mode, and that in (20d) is over elements adjacent to *both* ith and jth nodes. This is due to the fact that the nodal shape function N_j is nonzero only in those elements adjacent to the jth node of the scatterer. Therefore, both E and F are sparse matrices.

Partition the nodal field vector Φ in (20a) into two vectors: boundary nodal vector Φ^b and interior nodal vector Φ^i. Partition the E and F matrices accordingly and rewrite (20) as

$$E^{bb}\Phi^b+E^{bi}\Phi^i+F^b\Psi^b=S^b$$
$$E^{ib}\Phi^b+E^{ii}\Phi^i+F^i\Psi^b=S^i. \quad (21)$$

Then we are able to delete the interior nodal vector Φ^i from (21) and obtain an equation with only boundary variables

$$Y\Phi^b+Z\Psi^b=\tilde{S}, \quad (22)$$

where

$$Y=E^{bb}-C^{bi}E^{ib}, \qquad Z=F^b,$$
$$\tilde{S}=S^b-C^{bi}S^i, \qquad C^{bi}=E^{bi}(E^{ii})^{-1} \quad (22a)$$

C. *Combination of Global and Local Operators—Boundary Elements*

Applying Green's theorem to the exterior of the scatterer in Fig. 1, we obtain

$$\left[\int_B\frac{\partial}{\partial n}\phi^e(\mathbf{r})\,g(\mathbf{r},\mathbf{r}_B)\,dr_B-\oint_B\phi^e(\mathbf{r})\frac{\partial}{\partial n}g(\mathbf{r},\mathbf{r}_B)\,dr_B\right]+\int_{V^e}s^e(\mathbf{r}')\,g(\mathbf{r},\mathbf{r}')\,dV(\mathbf{r}')=\begin{cases}\phi^e(\mathbf{r}), & \mathbf{r}\in V^e\\ \frac{1}{2}\phi^e(\mathbf{r}), & \mathbf{r}\in B\\ 0, & \mathbf{r}\in V^i,\end{cases} \quad (23)$$

where B and V^i represent the boundary and interior of the scatterer, respectively, V^e denotes the exterior of the scatterer, $\mathbf{n}$ is the normal vector to the bounday (see Fig. 1), and g is the exterior Green's function (see Section III.A) of the waveguide, where ρ and k are constants. The two boundary integrals on the left-hand side of (23) are scattered fields due to the scatterer, and the volume integral is the direct field from the exterior source $s^e(\mathbf{r}')$. When the observer is on the boundary ($\mathbf{r} \in B$), the singular contribution of the second integral is extracted out explicitly and appears as the $\frac{1}{2}$ factor on the right-hand side of (23). Following the standard procedure of the boundary element method, (23) is discretized and becomes a matrix equation

$$[G^e \Psi^e + H^e \Phi^e] = S^e, \tag{24}$$

where the jth elements of vectors Ψ^e, Φ^e, and S^e are

$$\begin{aligned} \Psi_j^e &= \frac{\partial}{\partial n} \phi^e(\mathbf{r}_j), \\ \Phi_j^e &= \phi^e(\mathbf{r}_j), \\ S_j^e &= -\int_{V^e} s^e(\mathbf{r}')\, g^e(\mathbf{r}_j, \mathbf{r}')\, dV(\mathbf{r}'). \end{aligned} \tag{24a}$$

Here $\mathbf{r}_j$ is the mid-point of the jth boundary element ΔB_j. Similarly, the (ij)th elements of matrices G^e and H^e are

$$\begin{aligned} G_{ij}^e &= \int_{\Delta B_j} g(\mathbf{r}_i, \mathbf{r}_B)\, dr_B \\ H_{ij}^e &= -\int_{\Delta B_j} \frac{\partial}{\partial n} g(\mathbf{r}_i, \mathbf{r}_B)\, dr_B - \frac{1}{2}\delta_{ij}, \\ \delta_{ij} &= \begin{cases} 1, & i = j \\ 0, & i \neq j. \end{cases} \end{aligned} \tag{24b}$$

If the scatterer is non-penetrable, one does not need the finite element formulation in the previous section, and

$$\begin{aligned} \Psi^e &= (G^e)^{-1} S^e, \qquad \text{if} \quad \phi = 0 \\ \Phi^e &= (H^e)^{-1} S^e, \qquad \text{if} \quad \partial\phi/\partial n = 0. \end{aligned} \tag{25}$$

If the scatterer is penetrable, we have to convert the nodal values in Φ^b to the mid-point values in Φ^e, or vice versa, in order to equate the variables in (22) and (24). Assuming that the average value of the two nodal values of a boundary element is equal to the mid-point value, we obtain, from (22),

$$(\tilde{Y}\tilde{\Phi}^b + Z\Psi^b) = \tilde{S}, \tag{26}$$

where

$$\tilde{Y} = \tfrac{1}{2}(Y + Y') \tag{26a}$$

and Y' is a permutation of Y by moving the first column to the last column. Define a diagonal matrix

$$T = [t_{ii}]_{I \times I}, \qquad t_{ii} = \frac{\rho^e}{\rho^i(\mathbf{r}_i)}, \tag{27}$$

where r_i is the mid-point of the ith boundary element of the scatterer. Then (26) becomes

$$[\tilde{Y}\tilde{\Phi}^b + \tilde{Z}\tilde{\Psi}^b] = \tilde{S}, \tag{28}$$

where

$$\tilde{\Psi}^b = T\Psi^b, \qquad \tilde{Z} = ZT^{-1}. \tag{28a}$$

Solving (24) and (28) with boundary conditions $\tilde{\Phi}^b = \Phi^e$ and $\tilde{\Psi}^b = \Psi^e$, we will find the field and its normal derivative on the boundaries. Then from (21) or (23), we will be able to find the field in the exterior or interior, respectively, of the scatterer.

IV. STATIC LIMIT

Regarding the global operator, one must solve the Green's function problem of Poisson's equations subject to boundary conditions in a global medium. If the medium is range-independent, and by realizing that images, evanescent mode, and evanescent spectra in the static case are analogous to rays, modes (both evanescent and propagating), and spectra (both evanescent and propagating), respectively, one can apply the methods developed previously for the dynamic problems to the static problems.

An image representation is suitable for structures which have few layers, typically one or two. This is because a proliferation of images makes this representation impractical when the number of layers is large. This representation is only numerically efficient when the source and receiver are close to each other, compared to the overall dimensions of the structure within which they are placed.

The spectral integral has similar convergent properties as the image option, and synthesize the Green's function in terms of a superposition of evanescent spectra. This solution represents all of the images collectively and, therefore, can alleviate the difficulties of the image proliferations. However, the image solution is convenient for the separation of the dominant images, which experience fewer reflections and hence have a stronger contribution, from the rest of the images. This property is especially important when the source and receiver are overlapping each other, where the singular contribution due to the direct source has to be treated separately.

The modal solution represents the Green's function in terms of evanescent modes. Higher order modes die out

quickly when the source and receiver are widely separated, but are not negligible for a small separation. The convergent properties of the modal representation complement those of the previous two representations.

Similar to the ray–mode solution in the dynamic case, the modified image solution represents dominant image terms in closed form and we treat the rest of the images collectively as a remainder. This remainder, represented by a spectral integral may be evaluated by numerical integration along a fast convergent path through contour deformation in the complex-spectral domain. Unlike the dynamic case, there will be no poles intercepted by the contour deformation. This modified image option has the advantages of both image and spectral representations.

In principle, the static limit for the example given in Section III.A can be derived by letting the wavenumber k approach zero. The modal and the spectral integral representations maintain essentially the same forms as those in the dynamic case, respectively. The derivation of the image solution from the ray solution is not trivial. Solving (2) for $k=0$ by using the image method one has the image solution

$$g=\sum_{n=1}^{\infty}\sum_{l=0}^{4} g_{nl}^{0}, \qquad g_{nl}^{0}=\frac{-A_{nl}}{2\pi}\ln r_{nl} \tag{29}$$

with A_{nl} and r_{nl} specified in (4a). Though the image solution here has the same form as that of the ray solution (8), the one-to-one correspondence between g_{nl} in (4a) and g_{nl}^{0} in (29) does not exist. This is because each ln function in (29) exhibits a singularity as x approaches infinity. Therefore, each individual image term g_{nl}^{0} cannot have a Fourier integral representation as in (5) either. However, if one considers a complementary pair of images, i.e., their A_{nl}'s have different signs, the contribution of this pair converges to zero as x approaches infinity. Then, this pair of images can have a spectral representation. For example, consider the spectral integral of two conventional rays,

$$I(k,z)=g_{n1}+g_{n2}=\frac{-A_{n1}}{4\pi i}\int_{-\infty}^{\infty}\frac{1}{k} \times e^{i\kappa(z+2nd)+i\zeta(|x-x'|)}\left[e^{-i\kappa z'}-e^{i\kappa z}\right]d\zeta, \tag{30}$$

where we have assumed that $R_0=-1$ and then $A_{n2}=-A_{n1}$. By taking the derivative of $I(k,z)$ with respect to z to eliminate the $1/\kappa$ term in the integrand in (30) and making the static limit $k\to 0$, the spectral integral can be integrated analytically and is reduced to the following form:

$$\frac{dI(0,z)}{dz}=\frac{-A_{n1}}{2\pi}\left\{\frac{z+z'+2nd}{r_{n2}^{2}}-\frac{z-z'+2nd}{r_{n1}^{2}}\right\}. \tag{31}$$

By integrating (31), $I(0,z)$ becomes

$$I(0,z)=\frac{-A_{n1}}{2\pi}\ln\frac{r_{n1}}{r_{n2}}=g_{n1}^{0}+g_{n2}^{0}. \tag{32}$$

Thereby, we have accomplished the derivation of the image solution in the static case from the ray solution in the dynamic case. Note that the image solution in (29) for $R_0=R_d=1$ is not a valid representation because the series diverges. The modified image solution has the same form as that of the ray plus remainder solution if one replaces g_{nl} by g_{nl}^{0} and redefines the steepest descent contour C' of the remainder in (5) as

$$\frac{\mathrm{Im}(\zeta)}{\mathrm{Re}(\zeta)}=\pm\tan\left(\frac{|x-x'|}{2Nd}\right), \qquad \mathrm{Re}(\zeta)\lesseqgtr 0, \quad \mathrm{Im}(\zeta)\geqslant 0. \tag{33}$$

In a range-dependent medium, not every global operator for the dynamic responses is useful. Actually, the free space Green's function may be a convenient choice because the static field does not "propagate" and dies out within short ranges. Therefore, the need of a Green's function of the entire global environment is not so acute in a non-separable global environment as that in the dynamic case. An advantage of this approach is the simplicity of the Green's function; however, this requires the solution of a large system of simultaneous equations.

The static limit of the finite element method can be made by simply assigning zero to the k_e in (20d). Similarly, the mathematical formats for the static case of the boundary element method is exactly the same as those for the dynamic case. (The only difference is in the Green's functions, i.e., the global operator.) Therefore, the hybrid global and local operators are also applicable for problems governed by the Poisson equation.

V. NUMERICAL RESULTS

In the numerical simulation, the waveguide width and velocity are normalized to be one, and the boundary conditions at $z=0$ and $d\,(=1)$ are $\phi=0$. At first, we consider an inhomogeneous peanut-shaped scatterer in a waveguide excited by a line source (see Fig. 1). The four points on the interface of the scatterer denoted by a, b, c, and d are located at (0, 0.15), (0, 0.45), (0, 0.75), and (0.225, 0.52), respectively. The velocity of the inhomogeneous scatterer is described by $v(x)=(x+24)/18$, and the ρ quantities of the waveguide and the scatterer are chosen to be one. A line source is located at $(-0.25, 0.5)$. The magnitude of the wave

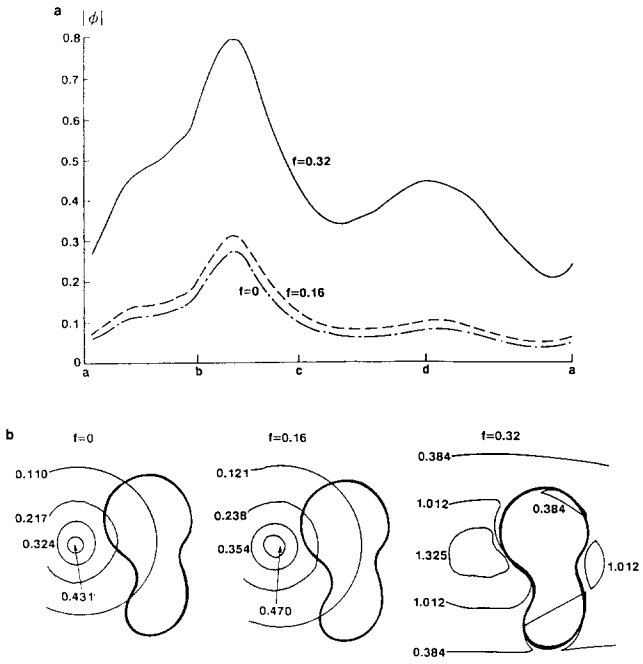

FIG. 2. The configuration employed for calculation is shown in Fig. 1: (a) $|\phi|$ along the boundary of the inhomogeneous scatterer verses boundary elements denoted clockwise from point a; (b) contour plots of $|\phi|$.

potential $|\phi|$ along the boundary of the peanut-shaped scatterer is shown in Fig. 2a for three frequencies ($f=0$, 0.16, 0.32 Hz), and the contour plot of $|\phi|$ is shown in Fig. 2b. At $f=0.16$ Hz, the field is still essentially static. But at 0.32 Hz, though the frequency is still low and no propagating mode exists in the waveguide yet, the field is substantially different from and is stronger than that in the static case ($f=0$). Second, we consider a waveguide with a deformed lower boundary defined by $z=0.125[1+\cos(4\pi x)]\,U(0.25-|x|)$, where U is the unit step function. The source is located at (0, 0.75). The three-dimensional plots and contour plots for three frequencies ($f=0$, 0.69, and 1.38 Hz) are shown in Fig. 3. In the static case ($f=0$), the waveguide has no propagating mode and has only a relatively small effect on the field distribution. For $f=0.69$ and $f=1.38$, the waveguide supports one and two propagating modes, respectively. From Fig. 3, one can see how the propagating modes are excited and interact with the deformed boundary. In the third numerical example, we consider a round impenetrable scatterer (with $\phi=0$ on its boundary) in a waveguide. The configuration is shown in the upper right corner of Fig. 4. The magnitude of the normal derivative of the wave potential along the boundary of the scatterer for three frequencies ($f=0$, 0.6, and 0.12 Hz) is also shown in Fig. 4. Observations similar to those for the second example can be made for this calculation. In all of these three examples, the hybrid ray–mode–boundary elements–finite elements method works well for both dynamic ($f\neq 0$) and static ($f=0$) cases. (Note that finite elements are not employed in the second and third examples because the scatterer is impenetrable.) The transition of physical quantities between dynamic and static regimes are very smooth. In Figs. 5a and b, we consider cylindrical rods of various shapes and locations in a parallel-plate structure. The rod is biased at constant potential and no external source is applied. The magnitude of the normal derivative of the wave

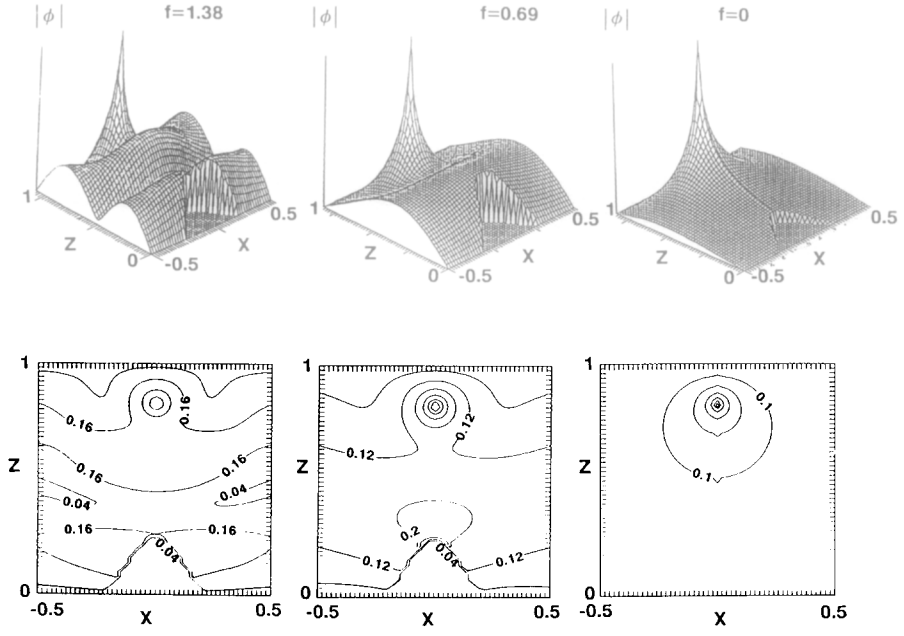

FIG. 3. The three-dimensional and contour plots of $|\phi|$ excited by a line source in a waveguide with a deformed lower boundary.

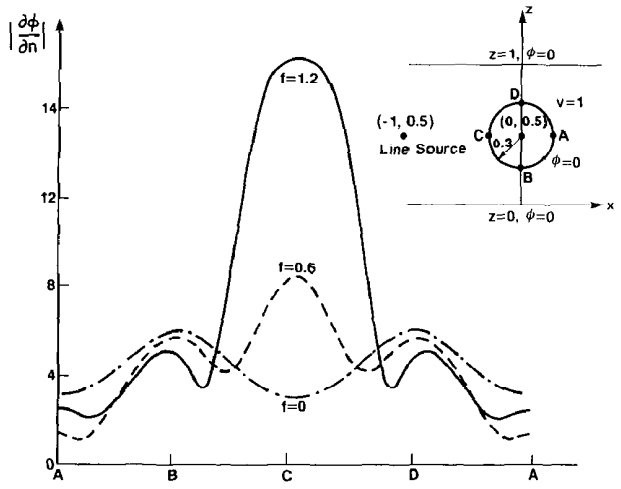

FIG. 4. The configuration employed for calculation is shown in the upper right corner, and $|\partial\phi/\partial n|$ along the boundary of the scatterer vs boundary elements denoted clockwise from point A is shown.

potential along the surface of the rod is shown in Fig. 5c. The effects of the location and shape of a scatterer on the field distribution is well demonstrated by this example. Once again, we see the hybrid global and local operators method efficiently solve static problems.

VI. CONCLUSION

We have demonstrated in principle and by specific examples how one can combine efficient global operators and flexible local operators in the same framework for solving both Helmholtz and Poisson equations in a complex environment. More reliable and efficient algorithms for more complex environments are to be developed. Since no rigorous solution is available, a hybrid combination of various methods should still be the best approach. To construct a hybrid scheme, the first step is to specify the applicable parameter regimes and to quantify the numerical efficiency and error of each individual method to be employed. (These aspects are still missing for many widely employed methods such as parabolic equation, beam shooting, local mode, etc.) The second step is to determine a combining strategy which indicates a priori where to employ a certain method and how to combine various methods together. The decision making process has to be hybrid method becomes a numbers game.) The last step is to have an overall assessment of various aspects (such as applicable ranges, errors, efficiency, compatibility with other methods) of the hybrid scheme. To make an algorithm robust and useful, this is a crucial step. In conclusion, to develop new hybrid schemes for unsolved problems and to make these new algorithms robust and efficient are the future directions.

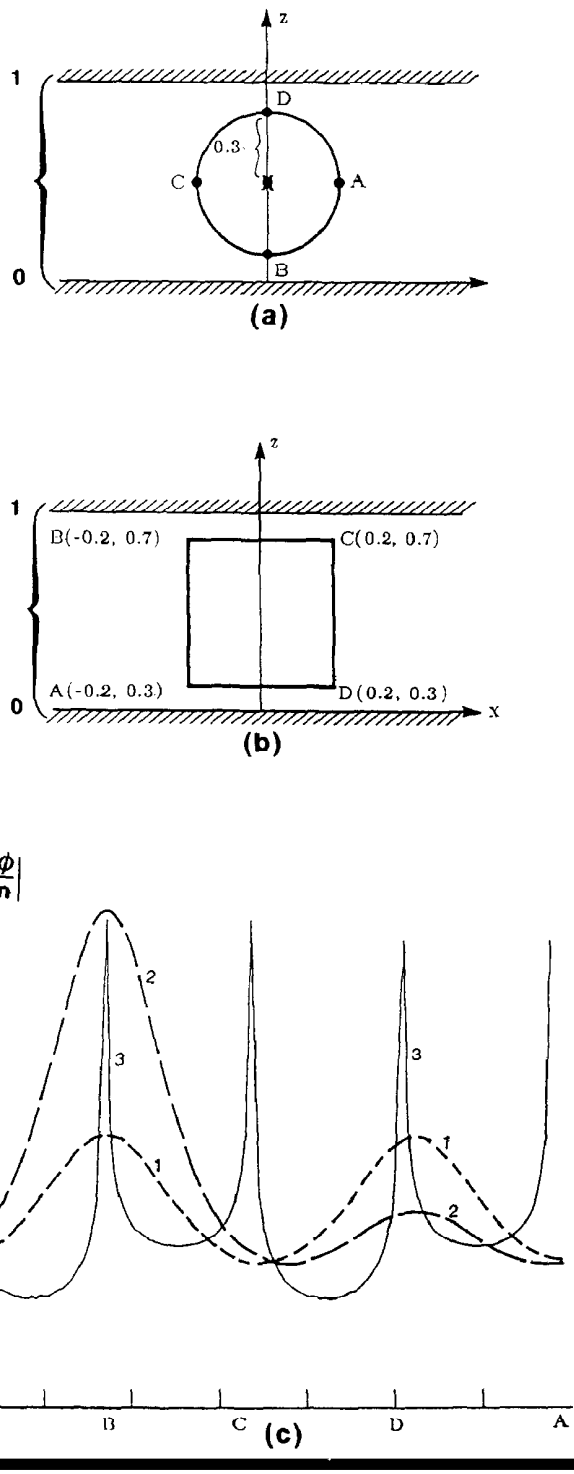

FIG. 5. The configuration employed for calculation is shown in a, b, and $|\partial\phi/\partial n|$ along the boundary of the scatterer vs boundary elements denoted clockwise from point $A$is shown in c: (a) A round rod with radius 0.3 centered at (0, 0.5) and (0, 0.4) two locations. (b) A square rod with four corners denoted by A, B, C, and D which are located at $(-0.2, 0.3)$, $(-0.2, 0.7)$, $(0.2, 0.3)$, and $(0.2, 0.7)$, respectively. (c) $|\partial\phi/\partial n|$ on the rod in Figs. a and b. curve 1, for the configuration in Fig. 5a when the round rod is centered at (0, 0.5); curve 2, for the configuration in Fig. 5a when the round rod is centered at (0, 0.6); curve 3, for the configuration in Fig. 5b.

APPENDIX A: EVALUATION OF THE REMAINDER IN (5)

We define a numerical distance, which measures the "distance" between the saddle point ζ_{sN} of (6a) and the mth modal eigenvalue ζ_m in (4b), as $D_{Nm} = P(\zeta_{sN}) - P(\zeta_m)$. If

$$|D_{Nm}| > 5 \qquad \text{for every } m \tag{A1}$$

and

$$N \geqslant \max\left\{\frac{3\,|x-x'|}{d}, 5\right\}, \tag{A2}$$

(5) can be approximated by the non-uniform stationary phase asymptotics:

$$R_N \approx \left[\frac{2\pi}{|P''(\zeta_s)|}\right]^{1/2} A(\zeta_s) \exp\left(iP(\zeta_s) - i\frac{\pi}{4}\right). \tag{A3}$$

Here, the condition in (A1) is to ensure that no pole is near the saddle point and the condition in (A2) is to ensure that the amplitude term is slowly varying with respect to the phase. In most parameter regimes, (A1) and (A2) can be satisfied simultaneously for some small truncation numbers N. However, if it is not so, R_N can be evaluated by numerical integration along the steepest descent path or by uniform asymptotics in terms of the Fresnel integral.

ACKNOWLEDGMENTS

This work is supported in part by the National Science Foundation under Grant No. ECS-8707615 and by the Joint Services Electronics Program under Contract No. F49620-88-C-0075.

REFERENCES

1. A. H. Olson, J. A. Orcutt, and G. A. Frazier, *Geophys. J. R. Astron. Soc.* **85** (1983).
2. A. S. Alekseev and B. G. Milhailenko, *J. Geophys.* **48**, 161 (1980).
3. L. B. Felsen, I. T. Lu, and K. Naishadham, in *Proceedings, URSI EM Theory Symposium 1989, CONGREX AB, Sweden* (unpublished).
4. I. T. Lu and L. B. Felsen, *J. Acoust. Soc. Am.* **78**, 701 (1985).
5. I. T. Lu and Felsen, *Geophys. J. R. Astron, Soc.* **84**, 31 (1986).
6. S. A. Chin-Bing, in *Proceedings, second IMACS Symposium on Computational Acoustics, Princeton, Mar. 1989* (unpublished).
7. I. T. Lu and L. B. Felsen, in *Proceedings, Conference on Ocean Seismo-Acoustics*, edited by T. Akal and M. Berkson (Plenum, New York, 1986).
8. Cerveny, *J. Geophys. Res.* **58**, 44 (1985).
9. I. T. Lu, L. B. Felsen, and Y. Z. Ruan, *Geophys. J. R. Astron. Soc.* **89**, 915 (1987).
10. I. T. Lu and L. B. Felsen, *J. Acoust. Soc. Am.* **81**, 897 (1987).
11. D. Lee and J. Papadakis, *J. Acoust. Soc. Am.* **68**(5), 1482 (1975).
12. I. T. Lu and R. Olesen, *IEEE Trans. Microwave Theory Tech.* **38**(6), 782 (1990).
13. I. T. Lu, "A hybrid finite difference–boundary element–ray–mode method for solving transient wave phenomena," in preparation.
14. I. T. Lu, *J. Acoust. Soc. Am.* **86**(3), 1136 (1989).
15. I. T. Lu and H. K. Jung, *J. Acoust. Soc. Am.* **87**(3), 988 (1990).
16. I. T. Lu and B. L. Ma, "A hybrid ray-mode-moment method for wave scattering from an aperture coupled system," *Int. J. Numer. Modeling: Electron. Networks, Devices Fields* **3**, 171 (1990).
17. B. L. Ma and I. T. Lu, *J. Electromagn. Waves Appl.* **4**(4) 311 (1990).
18. I. T. Lu, L. B. Felsen, J. M. Klosner and C. Gabay, *J. Acoust. Soc. Am.* **88**(1), 496 (1990).